Applied Physics Letters

Exciton tuning and strain imaging in WS_2 supported on PDMS micropillars

Cite as: Appl. Phys. Lett. **121**, 253101 (2022); https://doi.org/10.1063/5.0130927
Submitted: 16 October 2022 • Accepted: 09 December 2022 • Published Online: 21 December 2022

Published open access through an agreement with Universidad del País Vasco Facultad de Ciencias Químicas

M. Sledzinska, P. Xiao, E. Puig Vilardell, et al.

COLLECTIONS

Paper published as part of the special topic on Phononics of Graphene, Layered Materials, and Heterostructures

openaccess

View Online Export Citation CrossMark

ARTICLES YOU MAY BE INTERESTED IN

Excitonic performance and ultrafast dynamics in defective WSe_2
Applied Physics Letters **121**, 083102 (2022); https://doi.org/10.1063/5.0098100

Exciton-polaritons of hBN/WS_2 heterostructure in cavity observed at room temperature
Applied Physics Letters **121**, 231106 (2022); https://doi.org/10.1063/5.0118834

Phonónics of graphene, layered materials, and heterostructures
Applied Physics Letters **122**, 070401 (2023); https://doi.org/10.1063/5.0144480


Characterizing nanostructures?
Learn about a new way to get high-quality data in a fraction of the time
Read the tech note
Lake Shore CRYOTRONICS

AIP Publishing

© 2022 Author(s).

Exciton tuning and strain imaging in WS_2 supported on PDMS micropillars

Cite as: Appl. Phys. Lett. **121**, 253101 (2022); doi: 10.1063/5.0130927
Submitted: 16 October 2022 · Accepted: 9 December 2022 ·
Published Online: 21 December 2022

M. Sledzinska,[1,a)] P. Xiao,[1] E. Puig Vilardell,[1,2] E. Chávez Angel,[1]
M. J. Esplandiu,[1] and C. M. Sotomayor Torres[1,3]

AFFILIATIONS

[1] Catalan Institute of Nanoscience and Nanotechnology (ICN2), CSIC and BIST, Campus UAB, Bellaterra, 08193 Barcelona, Spain
[2] Departamento de Física, Universidad Autónoma de Barcelona, Bellaterra, 08193 Barcelona, Spain
[3] ICREA, Passeig Lluis Companys 23, 08010 Barcelona, Spain

Note: This paper is part of the APL Special Collection on Phononics of Graphene, Layered Materials, and Heterostructures.

[a)] **Author to whom correspondence should be addressed:** marianna.sledzinska@icn2.cat

ABSTRACT

Since the raise of 2D materials, significant research has been dedicated to their strain-dependent electronic and mechanical properties. In this work, we studied exciton energies and low-frequency phonon modes in CVD-grown mono- and few-layer WS_2 transferred on PDMS micropillars. The modification of the band structure under strain was investigated by photoluminescence (PL) spectroscopy at room temperature. Machine learning (ML) methods were used to analyze the PL spatial maps and facilitate the spectral deconvolution. For monolayer (1L) WS_2, red shift in the exciton energy was detected as a function of the position, which was ascribed to the presence of residual strain. For three-layer (3L) strained WS_2, a significant increase in the PL intensity corresponding to direct (K–K) band transition together with a change of exciton energy was observed. From the PL spectra, strain distribution maps were extracted for both studied samples, which strongly resembled the ML clustering results. Finally, the low-frequency Raman modes of WS_2 were studied on both Si/SiO_2 and PDMS substrates and no significant change of their frequency was observed for the 3L-WS_2.

© 2022 Author(s). All article content, except where otherwise noted, is licensed under a Creative Commons Attribution (CC BY) license (http://creativecommons.org/licenses/by/4.0/). https://doi.org/10.1063/5.0130927

One of the most exciting properties of 2D transition metal dichalcogenides (TMDs) is that their electronic structure[1–3] and mechanical properties[4,5] can be tuned by external strain. At the same time, it is relatively easy to experimentally induce strain in those materials, either by atomic force microscopy tip,[6–8] in bending[1,9–12] or stretching[13] setup, by creating wrinkles[14,15] or by interactions with pre-patterned substrates.[16,17]

Among the 2D TMDs family, 1L-WS_2 has attracted considerable interest due to its unique properties such as PL quantum yield (up to 6%) higher than other 2D semiconductors (~1% for MoS_2)[18] and large exciton–trion binding energy.[19] Furthermore, due to the breaking of inversion symmetry and strong spin–orbit coupling in 1L-WS_2, the electronic states of the two valleys have different chiralities, which have recently been applied to a nanophotonic circuit that can unidirectionally route the valley indices of 1 L-WS_2.[20]

Tuning of the optical and electronic properties of WS_2 and other TMDs by strain has been investigated extensively both theoretically and experimentally, but to date, most of the studies have been realized on TMDs monolayers due to their direct bandgap.[9–11,21] With an increasing number of layers, the bandgap becomes indirect and, consequently, the PL quantum yield decreases significantly. Another drawback of the previous works is that the presented spectra were taken only from one point on the sample without considering the strain distribution in the whole flake.[3,9–11] The importance of strain distribution mapping was recently discussed by Wang *et al.*, who showed that WS_2 follows continuum mechanics on the microscale and strain generates a non-uniform bandgap distribution even in a single WS_2 flake placed on flexible polymer substrates.[22]

Raman and PL spectroscopies are fast, non-destructive techniques to study the impact of the strain on the optical properties. Moreover, they require little or no sample preparation, and can provide qualitative and quantitative maps of the chemical structure and composition of the sample. However, the analysis of each individual spectrum in large spectroscopical maps can be time consuming. Machine learning is a rapidly growing field that has shown great potential in several research areas due to its ability to detect patterns in complex or very similar datasets that humans would likely miss.[23] Additionally, rapid spectral clustering can be performed in seconds,

© Author(s) 2022

providing valuable features not present in the intensity maps that default spectroscopy setup software gives to the users.

In this work, we studied room temperature PL and Raman spectra of single- and few-layer CVD-grown WS_2, transferred on PDMS micro-pillars. We applied machine learning techniques, such as data clustering (k-means), to simplify processing of the datasets and fit them more accurately. We measured spatial distributions of the PL spectra and observed significant changes in the exciton peak intensity and energy as a function of the position. These maps were subsequently converted into strain maps. We show that such a procedure can be straightforwardly applied to detect strain in both single and few-layer TMDs. Finally, the low-frequency Raman mode of 3L-WS_2 was studied as a function of strain.

WS_2 was synthesised on Si/SiO_2 substrates using CVD from solid precursors at 900° C under constant Ar flow. The resulting samples consisted of large area monolayer and few layer triangles, as shown in Fig. 1(a). 1L-WS_2 has a direct bandgap located at the K-point in the Brillouin zone; therefore, it shows a strong A exciton peak (X^A) corresponding to the direct excitonic transitions at 1.97 eV. A trion (charged exciton, X^-) is present at 1.95 eV,[24] as shown in Fig. 1(b). The Raman spectrum of 1L-WS_2 shows the characteristic peaks corresponding to in-plane vibrational modes E_{2g} (Γ-point in the Brillouin zone) and 2LA (M), in plane A_{1g} (Γ) and their combinations [Fig. 1(c)].[25] High PL intensity of the as-grown samples together with the Raman spectrum confirms their high quality.

Subsequently, the flakes were water-transferred to plain and micropatterned PDMS substrates.[26] After transfer to plain PDMS, the PL intensity decreased considerably, and the energy of both X^A and X^- excitons increased to 2.03 and 1.99 eV, respectively, due to the charge transfer induced by interaction with PDMS [Fig. 1(b)].[27] With the increasing number of layers, we observe a significant decrease in the PL intensity, together with a redshift to 1.93 eV, corresponding to the direct (K–K)–indirect (Γ–K) bandgap transition.[15,18] The PL signal for samples thicker than the monolayer is strongly suppressed [Fig. 1(d)], and PL peaks from the PDMS substrate become visible. This is due to the fact that the PL quantum yield with respect to the monolayer is more than three orders and four orders of magnitude lower for the bilayer and trilayer, respectively.[18]

The freshly transferred 1L samples showed only X^A and X^- excitons; however, after some time (~1 week), an additional peak (X^D)

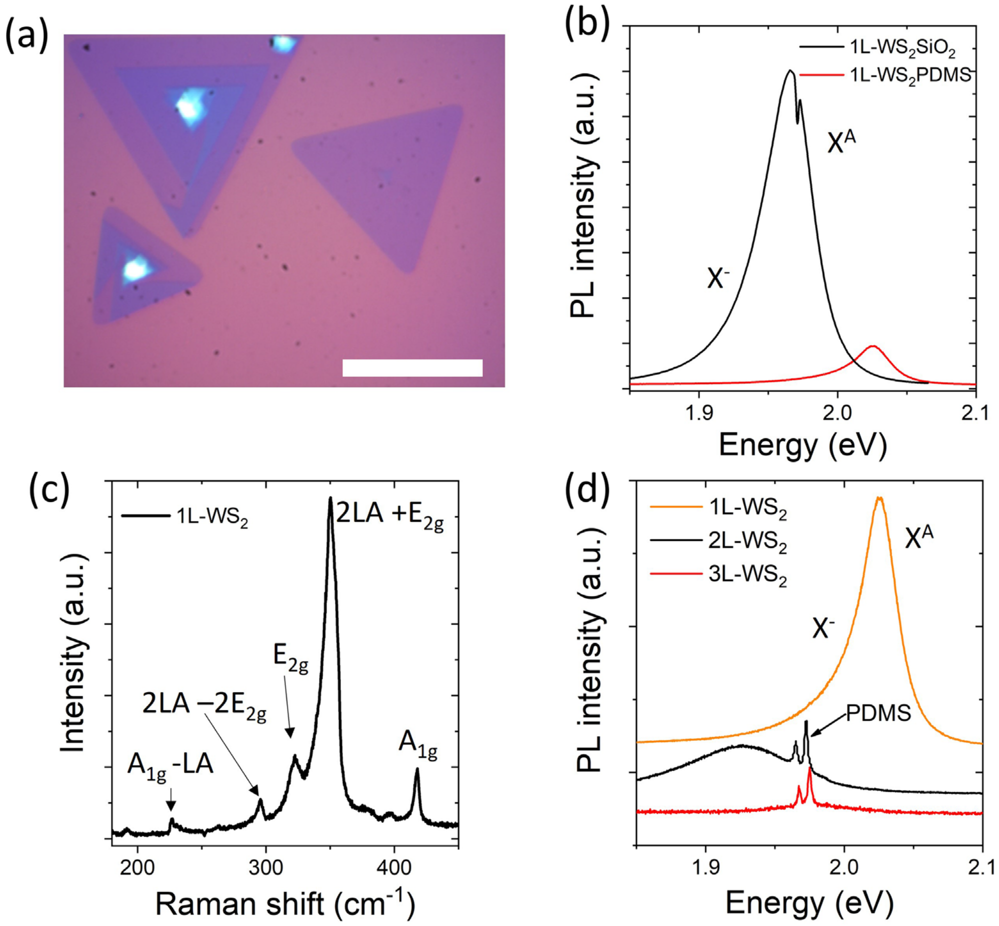

FIG. 1. Optical spectroscopy on CVD-grown WS_2. (a) Optical image of the WS_2 flakes synthesized on Si/SiO_2 substrates. Scale bar corresponds to 50 μm. (b) PL spectra of the as-grown and transferred to the PDMS substrate 1L-WS_2. (c) Raman spectrum of as-grown 1L-WS_2. (d) PL spectra of the 1, 2, and 3L-WS_2 on the PDMS substrate.

© Author(s) 2022

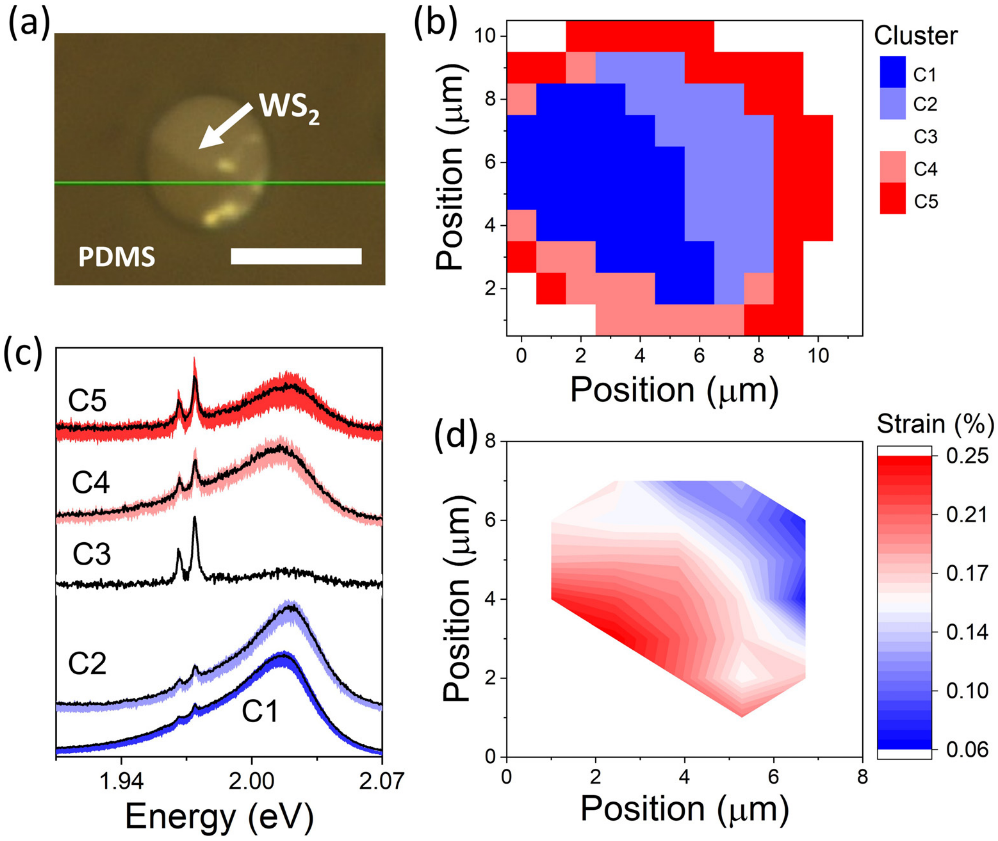

FIG. 2. 1L-WS$_2$ on the PDMS micropillar. (a) Optical image of the sample. Scale bar corresponds to 5 μm. (b) Clustering of the spectra, where clusters C1 and C2 correspond to spectra of WS$_2$ in the center of the pillar, C4 and C5 to pillar edges, and C3 to the background. (c) Examples of PL spectra from each cluster. The color outline corresponds to the standard deviation of spectra, and the black curve corresponds to the mean of the spectra in each cluster. (d) Strain distribution in the WS$_2$ layer.

located at 1.86 eV emerged in the PL spectrum (Fig. S1). It has been previously attributed to the presence of defects;[28] however, the origin of the peak in this sample is not fully clear. The defects could arise from the interaction between WS$_2$ and the environment, as it is known that 2D materials can easily degrade when in contact with air and moisture. The presence of defects did not affect the X^A and X$^-$ peaks, which remained at the energies of 2.02 and 1.99 eV.

For strain mapping experiments, the 1L-WS$_2$ was transferred to PDMS micropillars [5 μm diameter, 10 μm pitch, 5 μm height; Figs. 2(a) and S2]. The PL spatial map was taken from the area in Fig. 2(a) with 1 μm resolution. To facilitate the data analysis, we recurred to ML techniques, in particular, unsupervised learning. We used the k-means clustering algorithm to label samples based on features that group it with similar samples. Silhouette score contrasts average distance to elements in the same cluster with the average distance to elements in other clusters. As a rule, the higher the silhouette score, the value indicates that a given point is well matched to its own cluster and well separated from the neighbor clusters. For the raw spectra, the highest silhouette score was obtained for two clusters (Fig. S3). From the PL intensity map (Fig. S4) and cluster map (Fig. S3), it is clear that C1 and C2 roughly correspond to the background, and WS$_2$ supported on the pillar. After performing simple spectra preprocessing (baseline correction and peak area normalization), we further investigated higher number of clusters. In Figs. 2(b) and 2(c), the results for five clusters are shown. C1 and C2 correspond to the high-intensity spectra taken from the center of the pillar, C4 and C5 to pillar edges, and C3 to the background. Each cluster groups spectra of different PL energies. A similar analysis was also carried out using principal component analysis (PCA) as shown in the supplementary material. Figure S5 shows the maps of the scores of PC1 and PC2 as a function of the position in the sample. The PC1 score-map basically shows the difference between the spectra of WS$_2$, the edge, and the background. While the PC2 score-map is more sensitive to the strain difference in the WS$_2$ sample, other PCs does not show any significant information.

With the different clusters identified, we proceeded to fit the spectra. All the spectra except for the ones grouped in C3 (background) were fitted with a Lorentzian curve and a Gaussian curve for X^A and X$^-$ peaks, respectively. The energy distribution of X^A as a function of the position is shown in Fig. S6. It was previously reported that X^A energy scales linearly with strain as 46 meV/% strain for 1L-WS$_2$[9]. From this dependence, the strain map was calculated, as shown in Fig. 2(d). A small variation of strain between 0% and 0.3% was detected in the WS$_2$ layer. The highest strain was measured in the center of the pillar, at the edge of the WS$_2$ film, which is ascribed to the

© Author(s) 2022

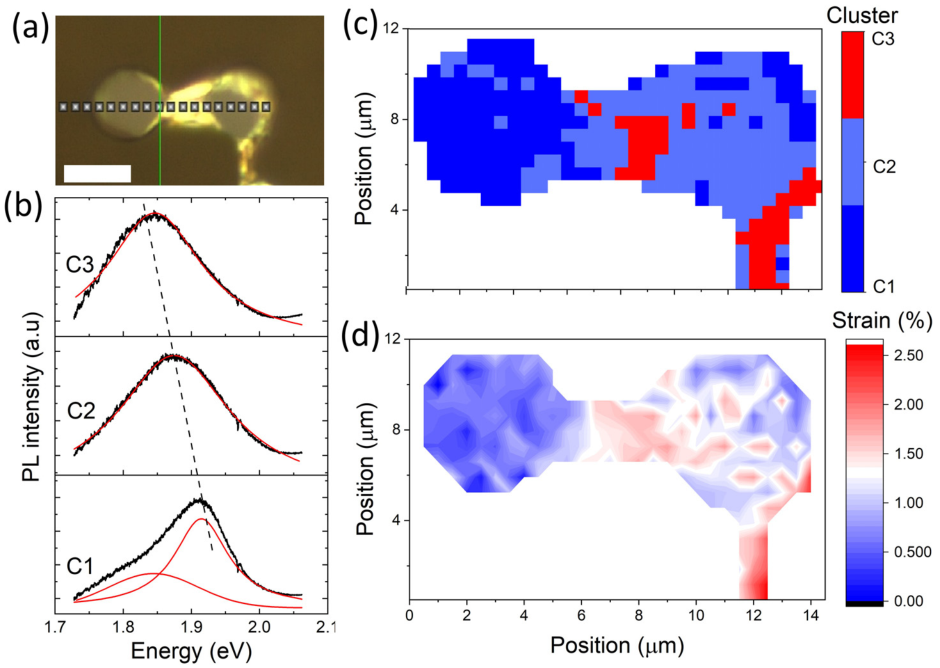

FIG. 3. 3L-WS_2 on the PDMS micropillar. (a) Optical image of the sample. Scale bar corresponds to 5 μm. (b) Clustering of the PL spectra. (c) Representative PL spectra from each cluster and corresponding peak deconvolution. (d) Strain distribution in the WS_2 layer.

residual strain coming from the transfer process. The maps in Figs. 2(b) and 2(d) strongly resemble each other; therefore, we can conclude that clustering algorithms could discern between spectra corresponding to different strain levels.

We further investigated few-layer WS_2 transferred to the same type of pillars [Fig. 3(a)]. By the optical contrast, we estimated the thickness to be 3L; however, the exact thickness of the sample is rather difficult to evaluate with optical methods. Contrary to other 2D materials, such as graphene,[29,30] when the thickness of TMDs is larger than 2L, Raman spectra closely resemble each other and cannot be used to confirm the exact thicknesses. The comparison between PL spectra of few-layer samples is typically difficult due to their low intensity. However, this sample showed enhanced PL signal from WS_2, which was much stronger with respect to the background PDMS signal than for 3L-WS_2 placed on plain PDMS [Figs. 3(b) and 1(d)]. The increase in the signal intensity corresponding to X^A excitons could be explained by the bandgap renormalization due to strain. According to density functional theory calculations, the tensile strain lowered the energy level of the conduction band valley and valence band hill at the K point of the Brillouin zone. This resulted in the conduction band at the K point aligned below the conduction band at the Λ point.[15] Therefore, we observed the indirect-direct bandgap transition for the strained samples and the intensity of the direct transition corresponding to X^A peak increased significantly. Interestingly, a significant increase in the PL intensity from the parts of the folded WS_2 layer was also measured [for example, in the region suspended between two pillars in Fig. 3(b)]. A similar increase was observed for wrinkled 2D materials and is an experimental evidence for the funneling of photogenerated excitons toward regions of a higher strain at the top of the wrinkle geometry.[14,15] For comparison, in the case of few-layer WS_2 suspended on pillars where no strain was present, such an increase in the PL intensities was not observed (Fig. S7).

We applied the k-means algorithm to cluster the spectra in the PL map, and the result is shown in Fig. 3(c). The highest silhouette score corresponds to the division into two clusters: background and WS_2 spectra, similarly as to the case of 1L-WS_2 discussed previously. The second highest score corresponds to four and five clusters, which differ only by a few points. Clusters C1–C3 correspond roughly to the left and right pillar and suspended (folded) WS_2 spectra, respectively. Representative spectra of each cluster are compared in Fig. 3(b). The spectrum corresponding to the left pillar can be fitted by two Lorentzian curves at 1.91 and 1.84 eV. The peaks can be assigned to direct (X^A) and indirect (X^I) band transitions. There is a clear trend of redshift in the X^A peak between the left and right pillars from 1.91 to 1.87 eV, respectively, a consequence of increasing strain. Furthermore, for the folded region, the peak shifts further to 1.85 eV.

Using clustering results, the spectra were fitted either by one or two curves, and the shift of X^A (50 meV/% strain[15]) was used to calculate the strain distribution, as shown in Fig. 3(d). The highest strain level (>2%) is present in the folded part of the sample, in agreement with previously reported studies.[15] WS_2 supported on the left pillar shows almost no strain (<1%), and WS_2 on the right pillar displays considerable amount of strain (1.5%–2%). Such non-uniform strain distribution is a result of the fabrication process, where the interaction between the 2D material and the transfer substrate is difficult to control. For industrial applications, when transferring large-area 2D materials for optical or optoelectronic devices, the presence of strain and the corresponding change in the electronic bandgap will be crucial for their correct operation. Noteworthy, the strain levels are adequately represented by clusters in Fig. 3(c). Therefore, we can use ML methods for detecting high-strain points in few-layer TMDs.

Finally, we investigated the low-frequency ($<100\,\text{cm}^{-1}$) phonon modes of this sample. These modes originate from motions of atomic layers instead of individual atoms and, therefore, are susceptible to

© Author(s) 2022

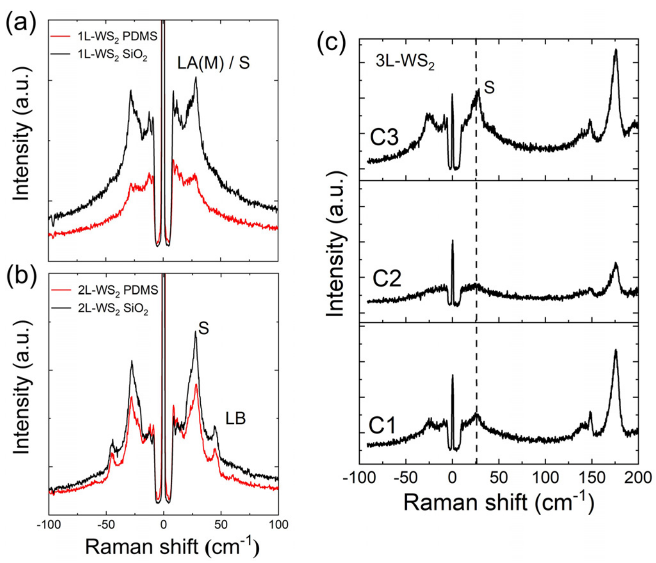

FIG. 4. Low frequency Raman spectra on the original Si/SiO$_2$ growth substrate and after transfer to PDMS for (a) 1L-WS$_2$ and (b) 2L-WS$_2$. (c) Low frequency Raman spectra of 3L-WS$_2$ corresponding clusters from Fig. 3(b) (from the bottom: C1: left pillar; C2: right pillar, and C3: suspended folded area).

interactions with surroundings such as substrate interactions or interlayer coupling in 2D materials.[31] For bulk WS$_2$, shear (S) and layer breathing (LB) modes are present at 27.5 and 47.8 cm^{-1}.[32] These modes are not expected for 1L samples, as they require the interaction of at least two layers. Accordingly, the S and LB modes were not detected for 1L TMDs with an exception of WS$_2$, where the low-frequency phonon mode at ~27.0 cm^{-1} was measured.[33] It has been tentatively assigned to LA (M); however, its origin in still not fully understood. In the study by Xiang *et al.*, the mode was recently attributed to the out-of-plane motion of tungsten and sulfur atoms, and it was explained as an interaction between WS$_2$ and the substrate in the CVD-grown WS$_2$.[34] Contrary to the work of Xiang *et al.*, we observed clear signature of the LA (M) mode for 1L-WS$_2$ for the as-grown sample on Si/SiO$_2$ and after the transfer to PDMS. This may suggest strong interaction between WS$_2$ and PDMS and could enable novel studies of low frequency modes in monolayers on flexible substrates.

For 2L-WS$_2$, we observed both S and LB modes on the growth substrate and after transfer to PDMS [Fig. 4(b)]. In the case of 3L-WS$_2$, we measured the S mode for both PDMS-supported and suspended samples. Spectra corresponding to different clusters, as in Fig. 3(b), are compared in Fig. 4(c). No detectable difference in the peak frequency was observed in the strain range of 0%–2.5% from which we can conclude that for few-layer WS$_2$, the S mode is not sensitive to strain. In the folded regions, we observed a strong increase in the peak intensity in comparison with the central laser peak (Fig. 4, C3). Similar to the PL signal enhancement, we attribute it to electron funneling into the wrinkles.

In summary, we studied exciton energies and corresponding strain distributions for mono- and few layer CVD-grown WS$_2$ transferred on PDMS micropillars. We used clustering algorithms to group similar spectra with two main objectives. First, clustering facilitated the spectral deconvolution of the PL signal. Second, we were able to correlate the clusters with the strain maps calculated from the shift in the PL energies. In the case of 1L-WS$_2$ the algorithm was able to distinguish between the spectra which differed by only 0.3% strain and in the case of highly strained 3 L-WS$_2$, the clustering results strongly resembled the strain map.

Finally, we studied the strain dependence of the low-frequency Raman mode for the multilayer WS$_2$ and did not observe any frequency shift up to approximately 2.5% of strain, only a significant intensity increase for the highly strained regions. Our results confirm machine learning techniques together with PL and Raman spectroscopy can provide a useful, fast, and efficient tool to analyze 2D materials.

See the supplementary material for the details of the effect of aging of the sample on the PL signal and SEM images of the patterned PDMS substrates. For the 1L-WS$_2$ on the pillar, we show the PL intensity and energy distribution of the X^A exciton, clustering, and PCA analysis of the spectra. Finally, we show the PL spectra analysis for few-layer WS$_2$ suspended on pillars when no strain is present.

This work has been supported by the Severo Ochoa Program (No. SEV-2017-0706 funded by MCIN/AEI/10.13039/501100011033), by the Spanish Ministry of Economy and Competitiveness (MINECO) under Contract Nos. PGC2018-095032-B-I00 and PID2021-124568NB-I00, and by the CERCA Programme/Generalitat de Catalunya. The authors acknowledge the European Union's H2020 FET Proactive Project TOCHA (Grant No. 824140) and the ERC-AdG Project LEIT (Grant No. 885689).

AUTHOR DECLARATIONS

Conflict of Interest

The authors have no conflicts to disclose.

Author Contributions

Marianna Sledzinska: Conceptualization (equal); Data curation (equal); Funding acquisition (equal); Investigation (equal); Visualization (equal); Writing – original draft (equal). **Peng Xiao:** Data curation (equal); Investigation (equal); Visualization (equal). **Eulalia Puig Vilardell:** Data curation (supporting); Formal analysis (supporting); Investigation (supporting); Visualization (supporting). **Emigdio Chávez-Ángel:** Formal analysis (equal); Methodology (equal); Visualization (equal); Writing – original draft (supporting). **Maria José Esplandiu:** Investigation (equal); Supervision (equal); Writing – review & editing (equal). **Clivia M. Sotomayor Torres:** Conceptualization (equal); Funding acquisition (equal); Supervision (equal).

DATA AVAILABILITY

The data that support the findings of this study are available from the corresponding author upon reasonable request.

REFERENCES

[1] F. Carrascoso, H. Li, R. Frisenda, and A. Castellanos-Gomez, Nano Res. **14**, 1698 (2021).
[2] C. D. Giorgio, E. Blundo, G. Pettinari, M. Felici, F. Bobba, and A. Polimeni, Adv. Mater. Inter. **9**, 2102220 (2022).

[3] A. Chaves, J. G. Azadani, H. Alsalman, D. R. da Costa, R. Frisenda, A. J. Chaves, S. H. Song, Y. D. Kim, D. He, J. Zhou, A. Castellanos-Gomez, F. M. Peeters, Z. Liu, C. L. Hinkle, S.-H. Oh, P. D. Ye, S. J. Koester, Y. H. Lee, P. Avouris, X. Wang, and T. Low, Npj 2D Mater. Appl. **4**, 29 (2020).

[4] B. Graczykowski, M. Sledzinska, M. Placidi, D. Saleta Reig, M. Kasprzak, F. Alzina, and C. M. Sotomayor Torres, Nano Lett. **17**, 7647 (2017).

[5] Y. Yoo, J.-H. Yang, and J.-H. Lee, Curr. Appl. Phys. **18**, 799 (2018).

[6] A. Castellanos-Gomez, M. Poot, G. A. Steele, H. S. van der Zant, N. Agraït, and G. Rubio-Bollinger, Nanoscale Res. Lett. **7**, 233 (2012).

[7] S. Bertolazzi, J. Brivio, and A. Kis, ACS Nano **5**, 9703 (2011).

[8] K. Bertoldi, V. Vitelli, J. Christensen, and M. van Hecke, Nat. Rev. Mater. **2**, 17066 (2017).

[9] X. He, H. Li, Z. Zhu, Z. Dai, Y. Yang, P. Yang, Q. Zhang, P. Li, U. Schwingenschlogl, and X. Zhang, Appl. Phys. Lett. **109**, 173105 (2016).

[10] H. J. Conley, B. Wang, J. I. Ziegler, R. F. Haglund, S. T. Pantelides, and K. I. Bolotin, Nano Lett. **13**, 3626 (2013).

[11] K. He, C. Poole, K. F. Mak, and J. Shan, Nano Lett. **13**, 2931 (2013).

[12] A. McCreary, R. Ghosh, M. Amani, J. Wang, K.-A. N. Duerloo, A. Sharma, K. Jarvis, E. J. Reed, A. M. Dongare, S. K. Banerjee, M. Terrones, R. R. Namburu, and M. Dubey, ACS Nano **10**, 3186 (2016).

[13] M. Sledzinska, G. Jumbert, M. Placidi, A. Arrighi, P. Xiao, F. Alzina, and C. M. Sotomayor Torres, ACS Appl. Electron. Mater. **2**, 1169 (2020).

[14] S. Deng, S. Che, R. Debbarma, and V. Berry, Nanoscale **11**, 504 (2019).

[15] K. P. Dhakal, S. Roy, H. Jang, X. Chen, W. S. Yun, H. Kim, J. Lee, J. Kim, and J.-H. Ahn, Chem. Mater. **29**, 5124 (2017).

[16] J. Chaste, A. Missaoui, S. Huang, H. Henck, Z. Ben Aziza, L. Ferlazzo, C. Naylor, A. Balan, A. T. C. Johnson, R. Braive, and A. Ouerghi, ACS Nano **12**, 3235 (2018).

[17] K. Wang, A. A. Puretzky, Z. Hu, B. R. Srijanto, X. Li, N. Gupta, H. Yu, M. Tian, M. Mahjouri-Samani, X. Gao, A. Oyedele, C. M. Rouleau, G. Eres, B. I. Yakobson, M. Yoon, K. Xiao, and D. B. Geohegan, Sci. Adv. **5**, eaav4028 (2019).

[18] L. Yuan and L. Huang, Nanoscale **7**, 7402 (2015).

[19] Z. Ye, T. Cao, K. O'Brien, H. Zhu, X. Yin, Y. Wang, S. G. Louie, and X. Zhang, Nature **513**, 214 (2014).

[20] Y. Chen, S. Qian, K. Wang, X. Xing, A. Wee, K. P. Loh, B. Wang, D. Wu, J. Chu, A. Alu, P. Lu, and C.-W. Qiu, Nat. Nanotechnol. **1**, 1178–1182 (2022).

[21] H. Shi, H. Pan, Y.-W. Zhang, and B. I. Yakobson, Phys. Rev. B **87**, 155304 (2013).

[22] F. Wang, S. Li, M. A. Bissett, I. A. Kinloch, Z. Li, and R. J. Young, 2D Mater. **7**, 045022 (2020).

[23] E. Chavez-Angel, B. Puertas, M. Kreuzer, R. Soliva Fortuny, R. C. Ng, A. Castro-Alvarez, and C. M. Sotomayor Torres, Foods **11**, 1304 (2022).

[24] K. F. Mak, K. He, C. Lee, G. H. Lee, J. Hone, T. F. Heinz, and J. Shan, Nat. Mater. **12**, 207 (2013).

[25] H. Zobeiri, S. Xu, Y. Yue, Q. Zhang, Y. Xie, and X. Wang, Nanoscale **12**, 6064 (2020).

[26] M. Sledzinska, B. Graczykowski, M. Placidi, D. S. Reig, A. E. Sachat, J. S. Reparaz, F. Alzina, B. Mortazavi, R. Quey, L. Colombo, S. Roche, and C. M. S. Torres, 2D Mater. **3**, 035016 (2016).

[27] B. Liu, W. Zhao, Z. Ding, I. Verzhbitskiy, L. Li, J. Lu, J. Chen, G. Eda, and K. P. Loh, Adv. Mater. **28**, 6457 (2016).

[28] P. K. Chow, R. B. Jacobs-Gedrim, J. Gao, T.-M. Lu, B. Yu, H. Terrones, and N. Koratkar, ACS Nano **9**, 1520 (2015).

[29] A. C. Ferrari, J. C. Meyer, V. Scardaci, C. Casiraghi, M. Lazzeri, F. Mauri, S. Piscanec, D. Jiang, K. S. Novoselov, S. Roth, and A. K. Geim, Phys. Rev. Lett. **97**, 187401 (2006).

[30] S. Sudhindra, F. Rashvand, D. Wright, Z. Barani, A. D. Drozdov, S. Baraghani, C. Backes, F. Kargar, and A. A. Balandin, ACS Appl. Mater. Interfaces **13**, 53073 (2021).

[31] X. Cong, X.-L. Liu, M.-L. Lin, and P.-H. Tan, Npj 2D Mater. Appl. **4**(1), 13 (2020).

[32] L. Liang, J. Zhang, B. G. Sumpter, Q.-H. Tan, P.-H. Tan, and V. Meunier, ACS Nano **11**, 11777 (2017).

[33] M. O'Brien, N. McEvoy, D. Hanlon, T. Hallam, J. N. Coleman, and G. S. Duesberg, Sci. Rep. **6**, 19476 (2016).

[34] Q. Xiang, X. Yue, Y. Wang, B. Du, J. Chen, S. Zhang, G. Li, C. Cong, T. Yu, Q. Li, and Y. Jin, Nano Res. **14**, 4314 (2021).

© Author(s) 2022